Progr Colloid Polym Sci (2006) 133: 35–40
DOI 10.1007/2882_048

Published online: 6 May 2006

Ingo Berndt
Jan Skov Pedersen
Peter Lindner
Walter Richtering

Structure of Doubly Temperature Sensitive Core-Shell Microgels Based on Poly-*N*-Isopropylacrylamide and Poly-*N*-Isopropylmethacrylamide

Ingo Berndt · Walter Richtering (✉)
Institute of Physical Chemistry,
RWTH Aachen University, Landoltweg 2,
52056 Aachen, Germany
e-mail: richtering@rwth-aachen.de

Jan Skov Pedersen
Department of Chemistry,
University of Aarhus, Langelandsgade 140,
8000 Aarhus C, Denmark

Peter Lindner
Institut Laue-Langevin,
6, rue Jules Horowitz,
BP 156-38042 Grenoble Cedex 9, France

Abstract Swelling properties of doubly temperature sensitive core-shell microgels consisting of two thermosensitive polymers namely poly-*N*-isopropylacrylamide (PNIPAM) with a lower critical solution temperature (LCST) at ca. 34 °C and poly-*N*-isopropylmethacrylamide (PNIPMAM) with a LCST of ca. 44 °C have been investigated by small-angle neutron scattering (SANS). Two types of microgels with different core-shell composition were studied: PNIPAM-core – PNIPMAM-shell microgels as well as a microgel with inverse structure, i.e. PNIPMAM-core – PNIPAM-shell. A core-shell form factor has been employed to evaluate the structure and the real space particle structure is expressed by radial density profiles. By this means the influences of composition and temperature on the internal structure have been revealed. At temperatures between the LCSTs the swelling of the PNIPMAM-shell leads to an expansion of the PNIPAM-core. At temperatures below the core LCST, the core cannot swell to its native size (i.e. in the absence of a shell) because the maximum expanded shell network prohibits further swelling. Thus depending on temperature the shell either expands or compresses the core. The inverse PNIPMAM-core – PNIPAM-shell microgel displays qualitatively different behavior. At intermediate temperatures, the segment density of the shell is higher as compared to the core. Since the density ratio of shell and core depends on temperature, such core-shell microgels provide interesting opportunities for encapsulation and controlled release.

Keywords Core-shell · Data modelling · Microgel · Poly-*N*-isopropylacrylamide (PNIPAM) · Poly-*N*-isopropylmethacrylamide (PNIPMAM) · Small angle neutron scattering (SANS)

Introduction

Materials composed of chemically cross-linked polymers that are sensitive to external stimuli have been used in a wide variety of applications as, e.g. in catalysis [1], drug delivery [2], sensors [3], biomolecule immobilization [4], colloidal crystals [5], and micro-optics [6]. Poly-*N*-isopropylacrylamide (PNIPAM) is the most widely investigated temperature sensitive microgel system [7] and shows structural changes upon heating above the lower critical solution temperature (LCST) in aqueous solution [8]. The temperature sensitive properties of PNIPAM can be extended to react on further stimuli as, e.g. ionic strength [9], solvent composition [10], pH [11], and selec-

tive reaction [12] by copolymerization with monomers that show sensitivity to one of those stimuli.

Lyon and co-workers introduced multi-responsive microgels with a core-shell morphology preparing PNIPAM core-PNIPAM-*co*-acrylic acid shell microgels which are sensitive to temperature and pH [13]. Our group recently presented core-shell microgels composed of two temperature sensitive polymers, PNIPAM and poly-*N*-isopropylmethacrylamide (PNIPMAM) with LCST of 34 and 44 °C, respectively, in either core or shell [14].

Detailed knowledge of the internal microgel structure is important for their application in fields where particular properties are required. Scattering methods as small-angle neutron scattering (SANS), small-angle X-ray scattering (SAXS) as well as dynamic (DLS) and static light scattering (SLS) are powerful tools to explore the structure of macromolecules and have been successfully applied to microgels [15, 16].

Stieger et al. have been the first to apply a direct modelling approach to describe SANS data of PNIPAM microgels over a wide q-range (where $q = \frac{4\pi}{\lambda} \sin\frac{\Theta}{2}$ is scattering vector at wavelength λ and scattering angle Θ) [17]. They convoluted a homogeneous sphere form factor with a Gaussian obtaining density profiles that gradually decreased at the surface to describe the surface fuzziness at temperatures below the LCST. This particle structure agrees with studies revealing that the cross linker is consumed faster than the monomer [18]. The same model was applied to SLS data of PNIPAM microgels and it was demonstrated that a stepwise addition of cross linker during the synthesis leads to a more homogenous structure [19]. Boyko et al. combined a hard sphere form factor with the form factor of a randomly branched polymer to describe SANS data of temperature sensitive poly-*N*-vinylcaprolactam-*co*-*N*-vinylpyrrolidone microgels [**?**]

The mutual influence of core and shell swelling was observed with core-shell systems where both core and shell consist of swellable polymer networks [14, 21, 22]. Experiments by Lyon and co-workers employing fluorescence resonance energy transfer techniques (FRET) revealed that swelling properties of the core are affected by the shell and the phase transition temperature of the core shifted towards higher temperatures as the shell thickness increased. This technique also allows for a calculation of core-shell interface thickness [23, 24].

Our group recently established a form factor model to describe scattering data and analyze the structure of microgel particles with core-shell morphology [25–28]. The model accounts for an interpenetrating layer of core and shell network and a graded particle surface. Here we demonstrate what structural information on core-shell microgels can be obtained from SANS combined with direct data modelling. Data from PNIPAM-core – PNIPMAM-shell microgels as well as from a microgel with inverse structure, i.e. PNIPMAM-core – PNIPAM-shell will be discussed.

Experimental Section

The synthesis of the core-shell microgel particles has been described in detail previously [14, 26]. Specifications of the shell composition of PNIPAM-core – PNIPMAM-shell microgels are given in the sample name scheme, for example *CS-5/0.69*, where the first number denotes the molar percentage of cross linker monomer in the shell (omitting the units) and the second number gives the relative mass ratio $m_{\text{shell}}/m_{\text{core}}$ after purification (see below), where m_{shell} is the mass of the shell and m_{core} is the mass of the core. The samples were purified by repeated ultra-centrifugation, decantation of the supernatant and redispersion in deionized water. Dynamic light scattering experiments have been performed with a modified ALV goniometer setup. SANS experiments were carried out at the D11 beam line at the Institut Laue-Langevin (ILL) in Grenoble, France. ILL provided software $\text{GRAS}_{\text{ANS}}\text{P}$ was used for absolute calibration, background correction, and azimuthal averaging following standard procedures at the ILL. The microgels were investigated at mass concentrations of 0.2 wt % in D_2O.

Theory and Data Analysis

Small-angle neutron scattering experiments provide an intensity distribution $I(q)$ in reciprocal space as a function of momentum transfer q and real space information can be revealed from data analysis [29]. A convenient way to express the scattering intensity distribution of a sample is the introduction of the differential scattering cross section $\frac{\mathrm{d}\sigma(q)}{\mathrm{d}\Omega}$ as it is independent of the transmission and form of the sample. In general the differential scattering cross section may be expressed for a dispersion of spherically symmetric particles by

$$\frac{\mathrm{d}\sigma}{\mathrm{d}\Omega} = n\,P(q)S(q)\,, \tag{1}$$

where n is the number density of particles. $P(q)$ is the particle form factor that describes the structure of the particle and $S(q)$ is the structure factor. $P(q)$ is normalized so that $P(0) = \Delta\rho^2 V^2_{\text{polymer}}$, where $\Delta\rho$ is the scattering contrast of the polymer and V_{polymer} the volume of the polymer within the particle. The structure factor accounts for the interference of scattering from different particles. In the present paper we present only data obtained at high dilution (0.2 wt %); hence, inter-particle correlations can be neglected and $S(q) = 1$.

Microgel particles are expected to have an inhomogeneous structure with a fuzzy surface due to faster consumption of cross linker molecules during at the earlier stages of the synthesis [18]. As a consequence our model of the structure of core-shell microgels employs a profile like the one shown in Fig. 1, with a graded outer surface characterized by σ_{out}, and an interface between core and

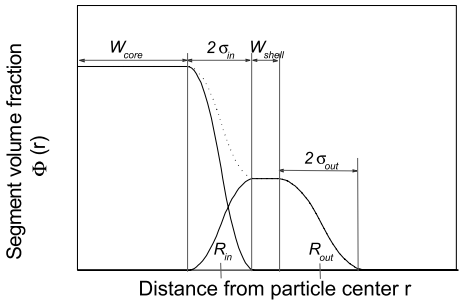

Fig. 1 Schematic illustration of the internal structure of core-shell microgels. W_{core} and W_{shell} describe the widths of central core and shell boxes. The interpenetration layer of core and shell is characterized by $2\sigma_{\mathrm{in}}$ and σ_{out} denotes the half width of the outer surface. The *dotted line* represents the total of core and shell

shell characterized by σ_{in}. The inner part of the core is described by a box of width W_{core} and the central part of the shell by a box of width W_{shell}. The central portions may have different densities depending on the swelling state of the particles. We used a parabolic shape for the fuzzy interfaces.

The radial density profile $\rho(r)$ of a particle with a graded surface can also be expressed by the half width radius R and the interface half width σ. The Fourier transformation of this profile can be calculated analytically and the normalized Fourier transformation is

$$\Phi(q,\,R,\,\sigma) = \frac{4\pi}{V}\left[\left(\frac{R}{\sigma^2}+\frac{1}{\sigma}\right)\frac{\cos\left(q(R+\sigma)\right)}{q^4} + \left(\frac{R}{\sigma^2}-\frac{1}{\sigma}\right)\frac{\cos\left(q(R-\sigma)\right)}{q^4} - \frac{3\sin\left(q(R+\sigma)\right)}{q^5\sigma^2} - \frac{3\sin\left(q(R-\sigma)\right)}{q^5\sigma^2} + \frac{2\cos(qR)}{q^5\sigma^2} + \frac{6\sin(qR)}{q^5\sigma^2}\right]. \quad (2)$$

Thus the scattering amplitude of a core-shell particle can be expressed by

$$A(q) = \Delta\rho_{\mathrm{shell}}V_{\mathrm{shell}}\Phi_{\mathrm{shell}}(q,\,R_{\mathrm{out}},\,\sigma_{\mathrm{out}}) + (\Delta\rho_{\mathrm{core}}-\Delta\rho_{\mathrm{shell}})V_{\mathrm{core}}\Phi_{\mathrm{core}}(q,\,R_{\mathrm{in}},\,\sigma_{\mathrm{in}})\,. \quad (3)$$

Particle size polydispersity was described by a normalized Gaussian number distribution. The finite collimation of the neutron beam, wave length spread, and the finite resolution of the detector contribute to the experimental smearing and can each be approximated by a Gaussian function [30] so that the experimental smearing can be expressed by a combined resolution function.

Results and Discussion

Core-shell microgels composed of PNIPAM, that exibits a LCST of 34 °C in the core, and PNIPMAM with a LCST of 44 °C in the shell show distinct changes in particle size at temperatures corresponding to the transitions of core and shell polymers. (All experiments were performed with D_2O as solvent; in H_2O the transition temperatures are slightly lower.) In Fig. 2 the temperature dependent hydrodynamic radius is plotted for a PNIPAM–PNIPMAM as well as for a PNIPMAM–PNIPAM core-shell microgel, the data of the corresponding core particles is shown for comparison.

The collapsed state at high temperatures can be regarded as a reference state since the synthesis proceeded at 70 °C, which is well above the core LCST and thus the shell is polymerized onto the collapsed core microgel. At temperatures above 45 °C all the core-shell particles have a larger radius as compared to the parent core.

PNIPAM-core – PNIPMAM-shell microgels reveal two transitions when the temperature is reduced. First the solvent quality changes from poor to good for the shell polymer and at 44 °C a distinct transition is found. With further decreased temperature below 34 °C the PNIPAM core starts swelling and a second transition is observed. For the inverse system PNIPMAM-core – PNIPAM-shell only a slight increase of the hydrodynamic radius is observed when lowering the temperature below the LCST of PNIPMAM. The core-shell microgel is smaller as compared to the naked core at temperatures between 35 and 41 °C.

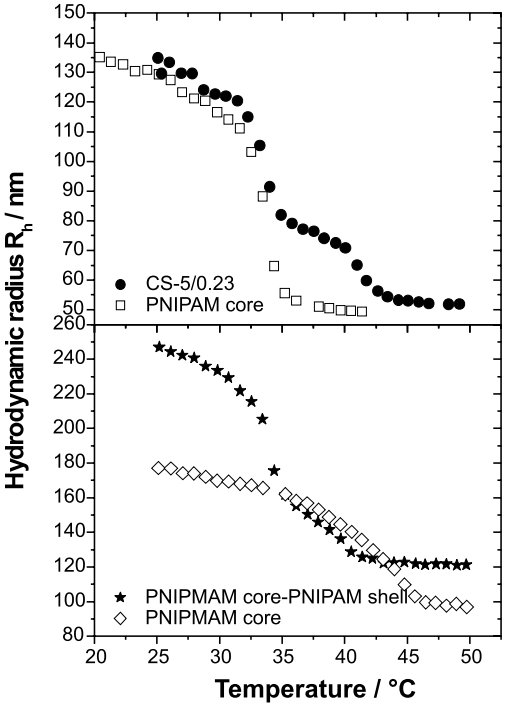

Fig. 2 Particle sizes as obtained from DLS in heavy water for core-shell microgels and the parent core. *Top*: PNIPAM-core – PNIPMAM-shell microgel sample CS-5/0.23, *bottom*: inverse PNIPMAM-core – PNIPAM-shell microgel

SANS is a powerful technique to investigate internal structural changes of core-shell microgels whereas DLS only provides information on the total hydrodynamic particle size. SANS experiments were carried out at three temperatures: 50, 39, 25 °C. These temperatures correspond to the states where (a) both core and shell are collapsed, (b) one part is swollen and the other is collapsed, and (c) both core and shell are swollen. A broad q-range (0.001–0.2 Å^{-1}) was studied which allows to obtain information on the internal as well as on the overall structure of the core-shell microgel particles.

PNIPAM-core – PNIPMAM-shell Microgels

The modeling of SANS data in the fully collapsed state is straightforward and the structure of the core-shell particles can be well described by two-box profiles with a narrow core-shell interface and a sharp outer surface. The width of the core-shell interfaces for the different samples is $2\sigma_{\text{in}} = 3.4$–$4.2$ nm and slightly smaller than the surface thickness of the collapsed pure core which is 5.4 nm. The width of the outer surface $2\sigma_{\text{out}} = 3.4$–$5.2$ nm is similar to that of the pure core. Increased shell/core mass ratios lead to thicker shells. The core profiles show only minimal deviations from the pure core profile. The total particle sizes quantitatively agree with the hydrodynamic radii as measured by DLS.

Behavior at intermediate temperature: In Fig. 3 scattering data and fits at 39 °C are presented. A slight shift of the form factor minima towards lower q-values is found with increased shell mass with samples CS-5/0.23, CS-5/0.69 and CS-5/1.42 indicating slightly increased dimensions of the dense PNIPAM core. Obviously, the scattering profile of sample CS-5/2.50 is more affected by contributions from the shell in the range $q = 0.015$–0.04 Å^{-1} and an even stronger shift to lower q is observed.

The scattering profiles reveal a steeper slope in the low q range ($q = 0.002$–0.008 Å^{-1}) with increased core-shell mass ratio indicating a bigger radius of gyration. This intuitively agrees with the DLS results as a thicker shell is more swellable than a thinner one. Furthermore, one observes that the slope of the scattering profiles in the intermediate q-range from 0.01–0.04 Å^{-1} becomes less steep with higher shell mass. Thus there are only small contributions from swollen shell $\left(I(q) \propto q^{-2}\right)$ to the scattering profile in this regime.

A swelling of the shell polymer network proceeds in tangential and radial direction. The radial swelling directly leads to an increase of the shell thickness. Swelling in the tangential directions influences the core as it leads to a mechanical stress at the core-shell interface [23, 25, 26]. This stress is released by expanding the flexible core and core-shell interface; in other words, the core-shell interface is pulled outwards. The force which is developed from the swollen shell to stretch the core increases with the shell

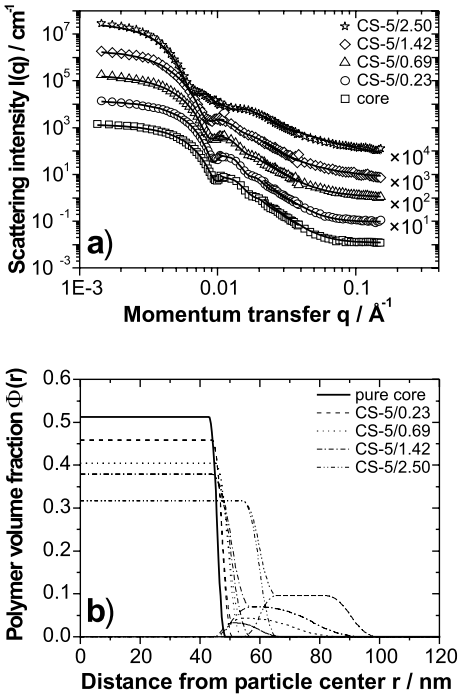

Fig. 3 **a** Scattering profiles of core-shell microgels with varied shell/core mass ratios taken at 39 °C. Samples CS-05/0.23, CS-5/0.69 and CS-5/1.42 exhibit a slight shift of the form factor minima towards lower q compared to the pure core indicating increased dimensions of the core. The scattering profile of CS-5/2.50 is more affected from contributions of the shell in the intermediate q range. **b** Density profiles at 39 °C. The PNIPAM core has a compact structure, but its dimension is increased due to the influence of the swollen shell. The effect increases with higher shell mass. *Dotted lines* represent the total polymer density distribution

mass [31, 32]. The core dimensions will be increased until equilibrium between the force exerted by the shell and the resisting elastic force developed in core is reached. Radial density profiles obtained from SANS curves at 39 °C are displayed in Fig. 3b.

Generally, the density profiles reveal that the structure can be described by a dense box profile for the core and a highly swollen shell. The dimensions of the core (described by R_{in}) grow from 47 nm to 60 nm as the shell mass increases and the width of the interface increases from $2\sigma_{\text{in}} = 7$ nm at the sample with the thinnest shell to 12 nm at the sample with the thickest shell. The polymer volume fraction of the core decreases from 46% to 32% in the same order. One observes that the volume fraction of the shell increase from 3.3 to 9.7% as the shell mass increases. The thickness of the shell as given by $\sigma_{\text{in}} + W_{\text{shell}} + 2\sigma_{\text{out}}$ increases from 20 to 39 nm.

The sample with the highest shell mass (CS-5/2.50) reveals a much broader box in the shell profile. This may explain why this sample shows a much larger stretching of the core. From a chemical point of view, one may assume a much higher cross linker gradient in the shell than

in the core, so that in case of thin shells (low shell mass) only a narrow layer of highly cross-linked polymer close to the core-shell interface is present and the fuzzy surfaces of the these samples mainly consist of only loosely cross-linked polymer chains. Only the cross-linked layers in the shell close to the core-shell interface will develop the force, which expands the core. Thus samples CS-5/0.23, CS-5/0.69 and CS-5/1.42 show small expansions of the core as the shell mass increases, but compared to sample CS-5/2.50 the deformations a rather small. Due to a much higher shell/core mass ratio CS-5/2.50 provides a much thicker layer of highly cross-linked polymer in the shell and will consequently develop a stronger expanding force than the other samples. Calorimetric measurements revealed that the core transition is shifted to higher temperatures when the swollen swell restrains the core to collapse. The temperature shift increases with the mass of the shell [31, 32].

Behavior at low temperature: The scattering data at 25 °C show fewer details as compared to higher temperatures. The total density profiles of all samples smoothly decay similar to the profiles of pure core microgels in the fully swollen state.

More remarkably for the PNIPAM-core – PNIPMAM-shell microgels is the fact that the dimensions of the core are significantly reduced to about 80–90 nm as compared to the naked core where $R_{in} + 2\sigma_{in}$ was found to be 122 nm. The situation at 25 °C is opposite to what happens at temperatures just below the shell's LCST. At 34 °C the core begins to swell and pushes the shell in radial direction and an opposing force is developed in the shell due to the elasticity of the network. The cross-links in the shell close to the core-shell interface limit the core swelling. Even stronger forces from the core cannot lead to further size increase when the shell network is expanded to a maximum extent. The cross-linker content is similar in all shells, so that one may understand why the reduced core swelling is almost independent of the shell mass.

PNIPMAM-core – PNIPAM-shell (Inverse) Microgel

Figure 4 displays the calculated radial density profiles obtained from SANS data on the inverse PNIPMAM-core – PNIPAM-shell microgel. At high temperatures, i.e. above both LCSTs, both core and shell are collapsed and the structure is well described by a density profile consisting of two boxes with a narrow interface and a sharp surface with a total width of 3–4 nm. The polymer volume fractions in core and shell are similar at ca. 50%. The particle size obtained from SANS agrees nicely with the hydrodynamic radius determined by dynamic light scattering. At 25 °C, both core and shell networks are swollen. The density profile still shows a change in the segment density between core and shell, and the profile decays constantly from the center to the periphery.

Most interesting is the density profile obtained at 39 °C. The dimensions of the core are increased due to the swelling of the PNIPMAM at this temperature and the water content in the core increased. Nevertheless, the dimensions of the core at 39 °C (128 nm) are still reduced as compared to the pure, naked core at 39 °C which were determined independently from SANS measurements to 148 nm (not shown in the plot). More important, however, the density of the shell is *higher* than the density inside the core. At this temperature D_2O is already a good solvent for the PNIPMAM core but still a bad solvent for the PNIPAM shell. Apparently, the thermodynamic hydration forces that lead to the swelling of the core are not sufficient to expand the PNIPAM network in the shell. Consequently, a structure is obtained with a shell that is *denser* as compared to the core. Thus the inverse PNIPMAM-core – PNIPAM-shell microgel shows a qualitatively different density profile as the PNIPAM-core – PNIPMAM-shell microgels discussed above.

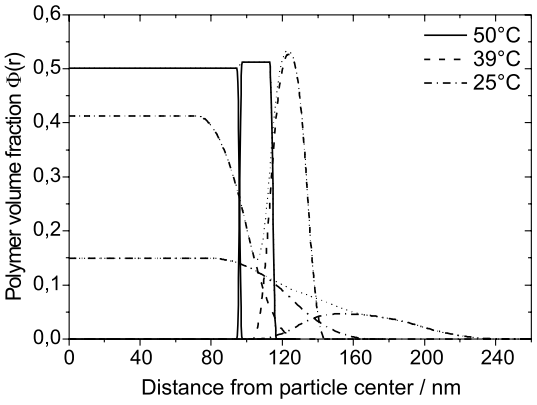

Fig. 4 Radial density profiles calculated from the modeling procedure at 25, 39, and 50 °C. At the intermediate temperature the shell reveals a higher density than the swollen core

Conclusions

The data presented here demonstrate how polymers with different temperature sensitivity can be combined in microgels with a core-shell morphology in order to tailor and control the polymer density in different regions of the particle. Most important is the sequence of polymer, i.e. whether the component with the higher transition temperature forms the core or the shell. In the former case, core-shell microgels with a higher density in the shell can be obtained. Since the density ratio of shell and core depends on temperature, such core-shell microgels provide interesting opportunities for encapsulation and controlled release.

Furthermore the temperature dependent swelling can be controlled by the shell-core mass ratio and the cross link density in core and shell. Depending on temperature and microgel composition, the shell can develop a mechanical force which expands the core or restricts its swelling.

This mutual influence can be studied in detail by scattering experiments that cover a broad q-range so that the entire particle structure is probed.

Acknowledgement Financial support by the Deutsche Forschungsgemeinschaft (DFG) and the Danish Natural Science Research Council is gratefully acknowledged.

References

1. Bergbreiter DE, Case BL, Liu Y-S, Caraway JW (1998) Macromolecules 31:6053–6062
2. Castro Lopez V, Raghavan SL, Snowden MJ (2004) React Funct Polym 58:175–185
3. Gerlach G, Guenther M, Suchaneck G, Sorber J, Arndt K-F, Richter A (2004) Macromol Symp 21:403–410
4. Cornelius VJ, Snowden MJ, Silver J, Fern GR (2004) React Funct Polym 58:165–173
5. Senff H, Richtering W (1999) J Chem Phys 111:1705–1711
6. Kim J, Serpe MJ, Lyon LA (2005) Angew Chem 117:1357–1360
7. Pelton R (2000) Adv Colloid Interf Sci 85:1–33
8. Heskins M, Guilett J (1968) Macromol Sci Chem A2(8):1441–1455
9. Rasmusson M, Vincent B (2004) React Funct Polym 58:203–211
10. Mielke M, Zimehl R (1998) Ber Bunsenges Phys Chem 102:1698–1704
11. Hoare T, Pelton R (2004) Macromolecules 37:2544–2550
12. Nayak S, Lyon LA (2004) Angew Chem 116:6874–6877
13. Jones CD, Lyon LA (2000) Macromolecules 33:8301–8306
14. Berndt I, Richtering W (2003) Macromolecules 36:8780–8785
15. Kratz K, Hellweg T, Eimer W (2001) Polymer 42:6631–6639
16. Saunders BR (2004) Langmuir 20:3925–3932
17. Stieger M, Richtering W, Pedersen JS, Lindner P (2004) J Chem Phys 120:6197–6206
18. Wu X, Pelton RH, Hamielec AE, Woods DR, McPhee W (1994) Colloid Polym Sci 272:467–477
19. Meyer S, Richtering W (2005) Macromolecules 38:1517–1519
20. Boyko V, Richter S, Grillo I, Geissler E (2005) Macromolecules 38:5266–5270
21. Jones CD, Lyon LA (2003) Langmuir 19:4544–4547
22. Jones CD, Lyon LA (2003) Macromolecules 36:1988–1993
23. Gan D, Lyon LA (2001) J Am Chem Soc 123:8203–8209
24. Jones CD, Mc Grath JG, Lyon LA (2004) J Phys Chem B 108:12652–12657
25. Berndt I, Pedersen JS, Richtering W (2005) J Am Chem Soc 127:9372–9373
26. Berndt I, Pedersen JS, Lindner P, Richtering W (2006) Langmuir 22:459–468
27. Berndt I, Pedersen JS, Richtering W (2006) Angew Chem 118:1769–1773
28. Berndt I, Pedersen JS, Richtering W (2006) Angew Chem Int Ed 45:1737–1741
29. Pedersen JS (1997) Adv Colloid Interf Sci 70:171–210
30. Pedersen JS, Posselt D, Mortensen K (1990) J Appl Crystallogr 23:321–333
31. Berndt I, Popescu C, Wortmann F-J, Richtering W (2006) Angew Chem 118:1099–1102
32. Berndt I, Popescu C, Wortmann F-J, Richtering W (2006) Angew Chem Int Ed 45:1081–1085